Close-Range Observations of Tornadoes in Supercells Made with a Dual-Polarization, X-Band, Mobile Doppler Radar

HOWARD B. BLUESTEIN, MICHAEL M. FRENCH, AND ROBIN L. TANAMACHI

School of Meteorology, University of Oklahoma, Norman, Oklahoma

STEPHEN FRASIER, KERY HARDWICK, FRANCESC JUNYENT, AND ANDREW L. PAZMANY*

Microwave Remote Sensing Laboratory, Department of Computer and Electrical Engineering, University of Massachusetts, Amherst, Amherst, Massachusetts

(Manuscript received 15 February 2006, in final form 26 April 2006)

ABSTRACT

A mobile, dual-polarization, X-band, Doppler radar scanned tornadoes at close range in supercells on 12 and 29 May 2004 in Kansas and Oklahoma, respectively. In the former tornadoes, a visible circular debris ring detected as circular regions of low values of differential reflectivity and the cross-correlation coefficient was distinguished from surrounding spiral bands of precipitation of higher values of differential reflectivity and the cross-correlation coefficient. A curved band of debris was indicated on one side of the tornado in another. In a tornado and/or mesocyclone on 29 May 2004, which was hidden from the view of the storm-intercept team by precipitation, the vortex and its associated "weak-echo hole" were at times relatively wide; however, a debris ring was not evident in either the differential reflectivity field or in the cross-correlation coefficient field, most likely because the radar beam scanned too high above the ground. In this case, differential attenuation made identification of debris using differential reflectivity difficult and it was necessary to use the cross-correlation coefficient to determine that there was no debris cloud. The latter tornado's parent storm was a high-precipitation (HP) supercell, which also spawned an anticyclonic tornado approximately 10 km away from the cyclonic tornado, along the rear-flank gust front. No debris cloud was detected in this tornado either, also because the radar beam was probably too high.

1. Introduction

Polarimetric radars have been used to discriminate among various types of hydrometeors, owing to their different shapes and composition (e.g., Zrnic and Ryzhkov 1999; Straka et al. 2000; Bringi and Chandrasekar 2001). It has been proposed that polarimetric radars can also distinguish between tornadic debris, which is assumed to consist of irregularly shaped and randomly oriented particles, and hydrometeors, which are more regularly shaped and more systematically oriented (Ryzhkov et al. 2005).

Ryzhkov et al. (2005), using S-band (10-cm wavelength) radars having half-power beamwidths of 1.9° by 0.9°, and 0.9° (the effective beamwidths are actually slightly wider, as a result of the rotation of the antenna), respectively, analyzed volume-scan data collected in supercells in central Oklahoma on 3 May 1999, 8 May 2003, and 9 May 2003, when tornadoes were reported at ranges of 45–60, 20, and 35–55 km, respectively. They found signatures of radar reflectivity factor Z between 45 and 55 dBZ and differential reflectivity (Z_{DR}) less than 0.5 dB, which they interpreted as representing debris. They also found relatively low values of the cross-correlation coefficient (ρ_{hv}) of less than 0.8. Although they argued that a ρ_{hv} signature might be the best indicator of a tornado signature because it is not affected by errors in radar calibration as Z_{DR} is, they also pointed out that ρ_{hv} might be in error if the differential phase varies within the radar resolution volume.

Beginning in 2001, a group from the School of Meteorology at the University of Oklahoma (OU) and a group from the Department of Electrical and Computer Engineering at the University of Massachusetts,

* Current affiliation: ProSensing, Inc., Amherst, Massachusetts.

Corresponding author address: Dr. Howard B. Bluestein, School of Meteorology, University of Oklahoma, 120 David L. Boren Blvd., Suite 5900, Norman, OK 73072.
E-mail: hblue@ou.edu

DOI: 10.1175/MWR3349.1

Amherst (UMass) operated a mobile, X-band (3-cm wavelength) radar for general storm surveillance and to probe tornadoes and tornadic storms at close range in the southern Great Plains. In spring, 2002, the radar first had polarimetric and Doppler capability (Pazmany et al. 2003). In spring, 2004, data were collected at close range in tornadoes on two days. In two instances, the tornado and its associated debris cloud and condensation funnel were clearly visible from the site of the radar.

The purpose of this paper is to detail the analyses of the polarimetric Doppler radar collected and to correlate them with visual aspects of the tornado, so as to determine if there is a debris signature that is distinguishable from a hydrometeor signature. This study extends that of Ryzhkov et al. (2005) in that more cases are added and in that an X-band radar was used; more importantly, the radar was located much closer to the tornadoes, so that the spatial resolution was finer. Also, since in some instances the tornado was visible, airborne debris could be correlated with features in the radar analyses. A description of the mobile radar system used and the way the data were collected and processed are detailed in section 2. Case studies for tornadoes on two days are discussed in section 3. The study is summarized and the major findings and implications are given in section 4.

2. Description of the mobile radar system and data collection

The mobile, polarimetric, X-band radar system (UMass X-Pol) was designed and built by graduate students and faculty at the Microwave Remote Sensing Laboratory (MIRSL) at UMass, as a less-expensive, lower power, yet reliable, polarimetric alternative to the Doppler on Wheels (DOW; Wurman et al. 1997). A polarimetric version of the DOW, the X-band Polarimetric radar on Wheels (X-POL), is used by the University of Connecticut (Anagnostou et al. 2004), but to the best of our knowledge, no analyses of tornadoes based on data from it have been reported in the literature. While UMass X-Pol is of great value in field experiments (e.g., Kramar et al. 2005), its design and construction was itself a valuable educational experience for the participating students at UMass. Like other ground-based mobile Doppler radars (Bluestein et al. 2001), it is mounted on a truck.

Details about the radar system are found in Pazmany et al. (2003) and Junyent et al. (2004). The radar system was developed from a magnetron-based marine radar transceiver manufactured by Raytheon. It was modified to transmit equal-power vertically (V) and horizontally (H) polarized pulses. Radar volumes were oversampled every 37.5 m (the radial resolution was actually 150 m) and then boxcar averaged over 75 m, every 37.5 m. A second receiver was added so that Z_{DR} and differential phase shift (K_{dp}) could be computed without having to use an expensive, high-power, transmit-receive switch. The cross-correlation coefficient ρ_{hv} and Doppler velocity are also computed, the latter being calculated from coherent-on-receive pulse-pair measurements.

Table 1. Characteristics of the UMass X-Pol.

Transmitter	
Center frequency	9.41 GHz
Peak power output	25 kW
Pulse width	1 μs (150-m range resolution)
Polarization	Equal power, simultaneous V and H
Pulse-repetition frequency	Staggered, 1.6–2 kHz
Max unambiguous velocity	± 60 m s^{-1}
Max unambiguous range	75 km
Antenna and pedestal	
Type (size)	Dual-polarized parabolic reflector (1.8 m)
Half-power (3 dB) beamwidth	1.25°
Gain	41 dB
Max scan rate	24° s^{-1} in azimuth and elevation
Receiver	
Dynamic range	70 dB
Noise figure	4 dB
Bandwidth	4.5 MHz
First IF	62.5 MHz
Second IF	2.5 MHz
Min detectable signal	−5 dBZ at 10 km

Since radars that operate in the X-band are highly susceptible to attenuation when there is heavy precipitation, it is anticipated that there could be errors in estimates of Z_{DR} when the radar beam passes through heavy rain, as a result of differential attenuation. While attenuation can be corrected for using, for example, the "self-consistent" method of Bringi et al. (2001), no attempts were made to do so in this study.

A staggered pulse repetition frequency was implemented to extend the maximum unambiguous velocity, while retaining a relatively long maximum unambiguous range (Zrnic and Mahapatra 1985). The radar transceiver, dual-polarized antenna, and pedestal are mounted on the truck platform; the data acquisition, positioner controller, and display systems are inside the crew cabin. Further details about the characteristics of the radar system are shown in Table 1.

The data processing system in 2004 allowed for two modes of data collection. In "surveillance mode," low data-rate radar reflectivity data only were displayed and recorded, potentially out to relatively long range

(as far as 120 km). In this mode, the radar operator could get a general idea of the intensity, size, shape, and locations of storms on a plan position indicator (PPI) display. In "data-collection mode," intermediate frequency (IF) radar data were streamed directly to disk for ranges out to 30 km. The data were not displayed in real time, owing to data bandwidth and processor limitations. The parameters H and V reflectivity (Z_H and Z_V), Z_{DR}, K_{DP}, ρ_{hv}, and Doppler velocity mean and standard deviation (Doviak and Zrnic 1984; Bringi and Chandrasekar 2001) were computed after field operations. Thus, surveillance mode was used when positioning the radar truck and in determining whether or not it was worthwhile to begin recording all the radar variables. During data collection (in both modes), the antenna scanned 360° at constant elevation angle. When raw data were being recorded, it was not possible to monitor any of the data on the PPI display. [Every 5 or 10 min or so, the radar operator would switch back to surveillance mode to ensure that the storm features being recorded were still noted on the PPI display at a desired range and azimuth; thus, there were many instances of several minute gaps in data collection (of *all* the radar variables).] Data were stored in wedge-shaped segments and for certain antenna-rotation speeds certain segments would not be stored, owing to aliasing. Finally, during 2004 the storage space on the radar computer was severely limited, so that at times older data would have to be deleted during field operations, in order to make room for new data, and therefore the radar operator had to be very conservative when making the choice to operate in data-collection mode. (The data-processing system was improved in 2005 and most of the aforementioned impediments to data collection have since been removed.) The processed data collected in both surveillance and data-collection modes were converted into a format compatible for use with the National Center for Atmospheric Research's (NCAR) SOLO software (Oye et al. 1995), so that radar images could be displayed, edited, and otherwise manipulated.

Field operations were conducted as in past years (Bluestein 1999; Kramar et al. 2005). Storms and tornadoes were scanned at an elevation angle as close to the ground as possible, but above most intervening trees, buildings, etc. Unlike the data collected by Ryzhkov et al. (2005) using fixed-site radars, the data collected by UMass X-Pol were usually less subject to beam blockage near the ground at azimuths along which tornadoes were located, owing to our efforts to keep the view of storm features as unobstructed as possible, thanks to the mobility of the radar truck. However, the antenna was not as elevated as the fixed-site S-band radars used by Ryzhkov et al. (2005) were, and no efforts were made to correct for any blockage at all as they had done. Also, efforts were not made to level the radar truck, so there may be some unknown amount of vertical excursions in the PPI scans. The antenna rotation speed was as rapid as possible so that the data were oversampled in azimuth just enough that there was at least one beam for every 1.25° in azimuth.

In addition to the data collected by UMass X-Pol, data were also collected by the UMass millimeter-wavelength (W-band), mobile Doppler radar (Bluestein et al. 2005), by two DOWs (Kosiba et al. 2005), and by an infrared digital thermal camera (Tanamachi et al. 2006), analyses of which are reported elsewhere.

3. Case studies

a. Spatial resolution of the data collected in the cases

During the 2004 field experiment, which ran from late April to early June, data were collected in tornadoes at ranges varying from ~4 km on 12 May to ~8–14 km on 29 May. Resolution volumes therefore varied from slightly greater (taking into account smearing due to antenna rotation) than ~70 m × 70 m × 150 m on 12 May to slightly greater than ~175 m × 175 m × 150 m on 29 May.

The elevation angles of the antenna were approximately 2.5° and 3° on 12 May, and 5.1° and 4.8° on 29 May; thus, the approximate height of the center of the radar beam on 12 May was ~175–210 m AGL and on 29 May was ~675 m–1.25 km AGL. Since the radar platform was not leveled, the aforementioned heights could be in error to an unknown extent. The higher heights of the beam on 29 May were a product of the longer range to the tornado and the higher elevation angles, which were necessary so that the radar beam was aimed above distant trees. Since from experience we believe that the elevation angles could have been in error by as much as 2°, the uncertainty in the height of the center of the beam was ~±140 and ±450 m on 12 and 29 May 2004, respectively.

For comparison, the height of the center of the beam in the data presented by Ryzhkov et al. (2005), which was at 0° for data collected on 3 May 1999 and 0.5° elevation angle for data collected on 8 and 9 May 2003, varied from as low as ~30–175 m AGL when the tornado was at 20-km range to ~435 m AGL when the tornado was at 50-km range. Thus, the heights above the ground of their data were comparable to those of ours in two cases, but lower than ours in the other. The radial resolution of the data was 240 m on 3 May 1999

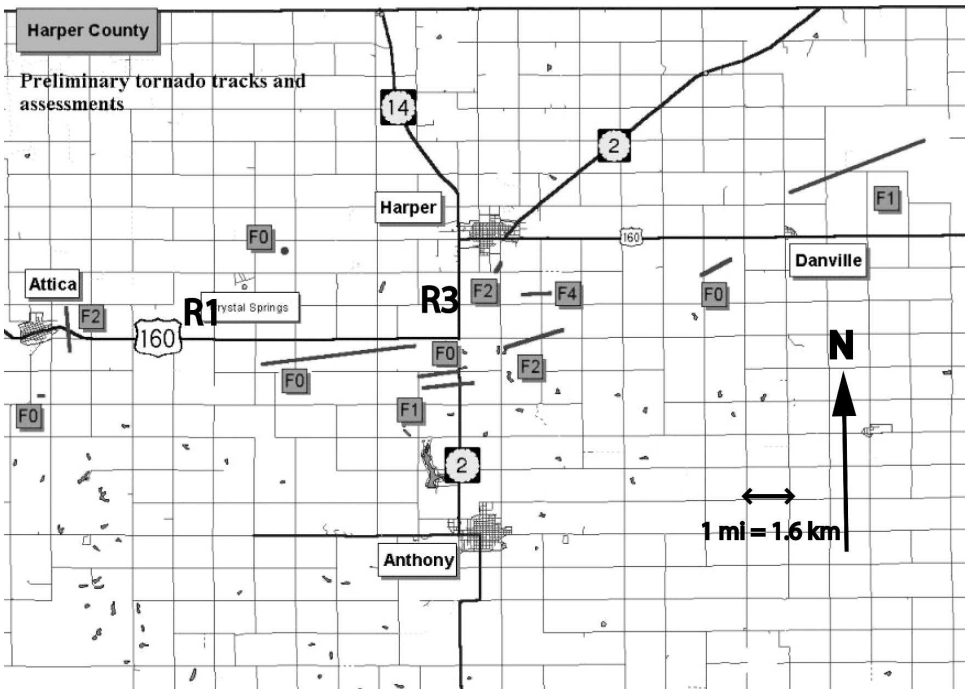

FIG. 1. Tornado tracks and estimated F-scale rating of each tornado on 12 May 2004, as determined by the NWS, Wichita, KS. Also shown are two of the deployment sites (R1 and R3) of the UMass mobile, X-band radar when data were being collected, for the second and fourth tornado.

and 267 m (A. Ryzhkov 2005, personal communication) on 8 and 9 May 2003. Thus, the resolution volumes of the data were, at best, ~315 m × 315 m × 265 m (on 8 May 2003). Thus, although most of the data collected by UMass X-Pol were at a much finer spatial resolution (~70 m × 70 m × 150 m on 12 May 2004), data were collected only at one elevation angle (as close to the ground as possible), while the data described by Ryzhkov et al. (2005) were collected in a deep volume. Thus, the dataset detailed in this paper lacks the vertical continuity nicely shown by them.

b. Tornadoes on 12 May 2004 in southern Kansas

1) THE "ATTICA" TORNADO

A supercell that formed in south-central Kansas, near the intersection of the dryline and an outflow boundary, around 1730–1800 CDT (UTC is 5 h later) on 12 May 2004, spawned a series of tornadoes (Fig. 1), two of which were probed in data collection mode by the UMass X-Pol. One tornado, which formed just east of Attica, Kansas, produced damage rated by the National Weather Service (NWS) as F2 (see Fujita 1981 for the Fujita scale). This tornado tracked to the north-northwest and was highly visible from the radar truck (Fig. 2), only ~4 km to its east. Owing to its motion normal to the road on which the radar truck was parked, the storm-intercept crew was able to remain at one location for the entire life of the tornado.

A storm-scale perspective of the radar reflectivity pattern of the 12 May supercell at the time of the Attica tornado (2001:09 CDT; times for radar images here and that follow are valid for the time of the beginning of the scan) is seen in Fig. 3c. A hook echo coiled up at its tip and a low-reflectivity notch north and northeast of the hook echo are connected to the main body of the storm, which lies to the north and northeast. Before the tornado had formed, an appendage of radar echo on the southwest side of the storm (~45 dBZ) narrowed into a thin band of much weaker radar reflectivity (Fig. 3a), which curved around in a counterclockwise manner, culminating in a narrow ring of a 30-dBZ echo; the band of weaker radar reflectivity then curved back around in a clockwise direction, giving the appearance of a ring having two spiral bands (Fig. 3b). It is likely that the ring marks the debris in what looked like a dust whirl on the ground (not shown), in advance of the development of the tornado. Neither polarimetric nor Doppler velocity data were available at this time. The appearance and horizontal dimensions of the ring looked very much like those of a dust devil (Bluestein et al. 2004a; cf. Fig. 4). The location of the ring was at

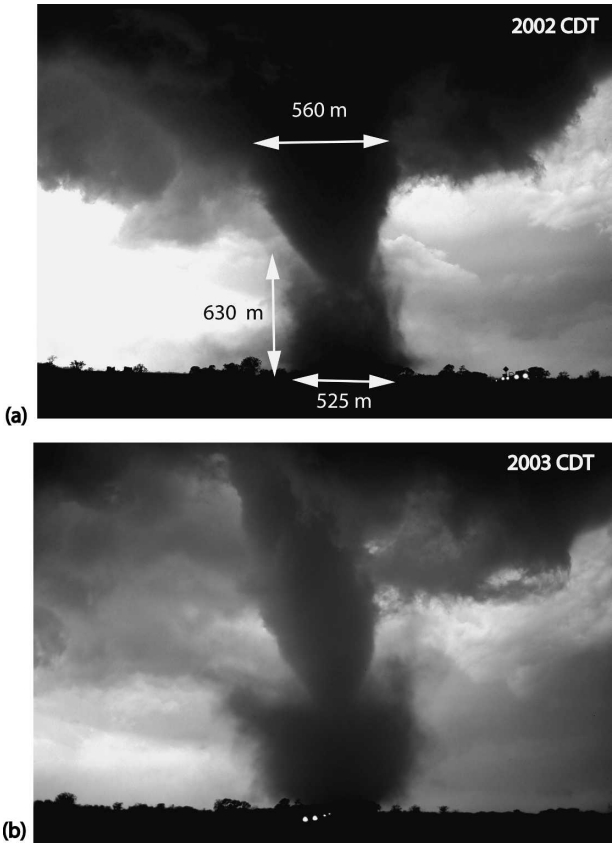

FIG. 2. Selected images of the Attica tornado, during its mature stage, at (a) 2002 and (b) 2003 CDT 12 May 2004. The view is to the west from a location approximately 5 km east of Attica, KS. The approximate dimensions of the opaque debris cloud, condensation funnel, and height of the cloud base, as determined from photogrammetric analysis, are as indicated. (Photographs courtesy of H. Bluestein.)

an inflection point along the line and probably marked the intersection of the hook echo with the rear-flank gust front, as in a tornado in Nebraska discussed by Bluestein et al. (2003; cf. Figs. 5 and 6) and in a tornado in Kansas discussed by Tanamachi et al. (2007).

The radar reflectivity pattern associated with the tornado was a ring of moderately intense echo (~40 dBZ) about 625 m in diameter, surrounding a weaker region of echo (~15–25 dBZ) ~200 m in diameter; beyond the ring of intense echo there were spiral bands of reflectivity of ~40–50 dBZ (Fig. 4a). Such features are common in tornadoes when viewed by radars at close range (e.g., Fujita 1981; Bluestein et al. 1993; Wurman et al. 1996; Wakimoto et al. 1996; Wurman and Gill 2000; Bluestein and Pazmany 2000; Bluestein et al. 2003, 2004b; Alexander and Wurman 2005; Dowell et al. 2005).

The region encompassing the ring of moderately intense echo was collocated with quasi-circular regions of relatively low Z_{DR} and ρ_{hv} (Fig. 4b). These regions of Z_{DR} below ~0.5 dB (coded green and white) and ρ_{hv} below 0.5 (coded green) were ~900 m in diameter. The first spiral band outside the inner ring was characterized by Z_{DR} of ~1.5–3 dB. The Doppler velocity couplet associated with the tornado vortex was ~325 m in diameter, while the diameter of winds in excess of ~25 m s^{-1} was ~800 m in diameter (Fig. 4c). While F2 damage was reported with this tornado, the relatively weak winds sensed by the radar may have been a result of the relatively high elevation angle, such that the center of the radar beam was ~175 m, well above the tops of nearby trees, and possibly above the level of the highest wind speed (e.g., Wurman and Gill 2000; Alexander and Wurman 2005; Bluestein et al. 2005). It also possible that the Doppler wind data displayed in Fig. 4c were not collected when the tornado was of F2 intensity. The wind speeds measured by UMass X-Pol were consistent with those measured by DOW3 (more information available online at www.cswr.org/dataimages/rotate/12May2004.html) at approximately the same time. To further illustrate how radar reflectivity, Z_{DR}, and Doppler velocity were correlated, the aforementioned parameters are plotted in Fig. 5 (ρ_{hv} is not shown) through the tornado, at the constant range of the center of the tornado. A region of negative values of Z_{DR} is clearly evident encompassing the core of the tornado at 2001:09 CDT; the ring of moderate reflectivity is less easily discernible. The extremely low values of Z_{DR} at the center of the vortex (<-2 dB) in the face of relatively high reflectivity (~30 dBZ) may indicate that that there were relatively few pieces of highly reflective debris there and that they were not randomly distributed.

From the known distance of the vortex signature from UMass X-Pol (and from the nearby UMass W-band radar) and still photographs of the tornado taken from the site of the radar truck, the dimensions of the visible dust/debris cloud and condensation funnel were estimated photogrammetrically (Fig. 2). The width of the most opaque portion of the symmetrical portion of the dust/debris cloud was ~525 m, while the dust/debris cloud also extended off to the south (to the left in Fig. 2) another 300 m or so. There is thus qualitative agreement between the visible dust/debris (cross-sectional diameter in the viewing plane of ~525–825 m), and the regions of low Z_{DR} and low ρ_{hv} that mark the tornado (cross-sectional diameter in the viewing plane of ~900 m), though the latter extends out farther than the ring of most intense echo (~625 m in diameter). The distance from the center of the tornado to the center of the ring of the most intense debris echo (~310 m) is greater

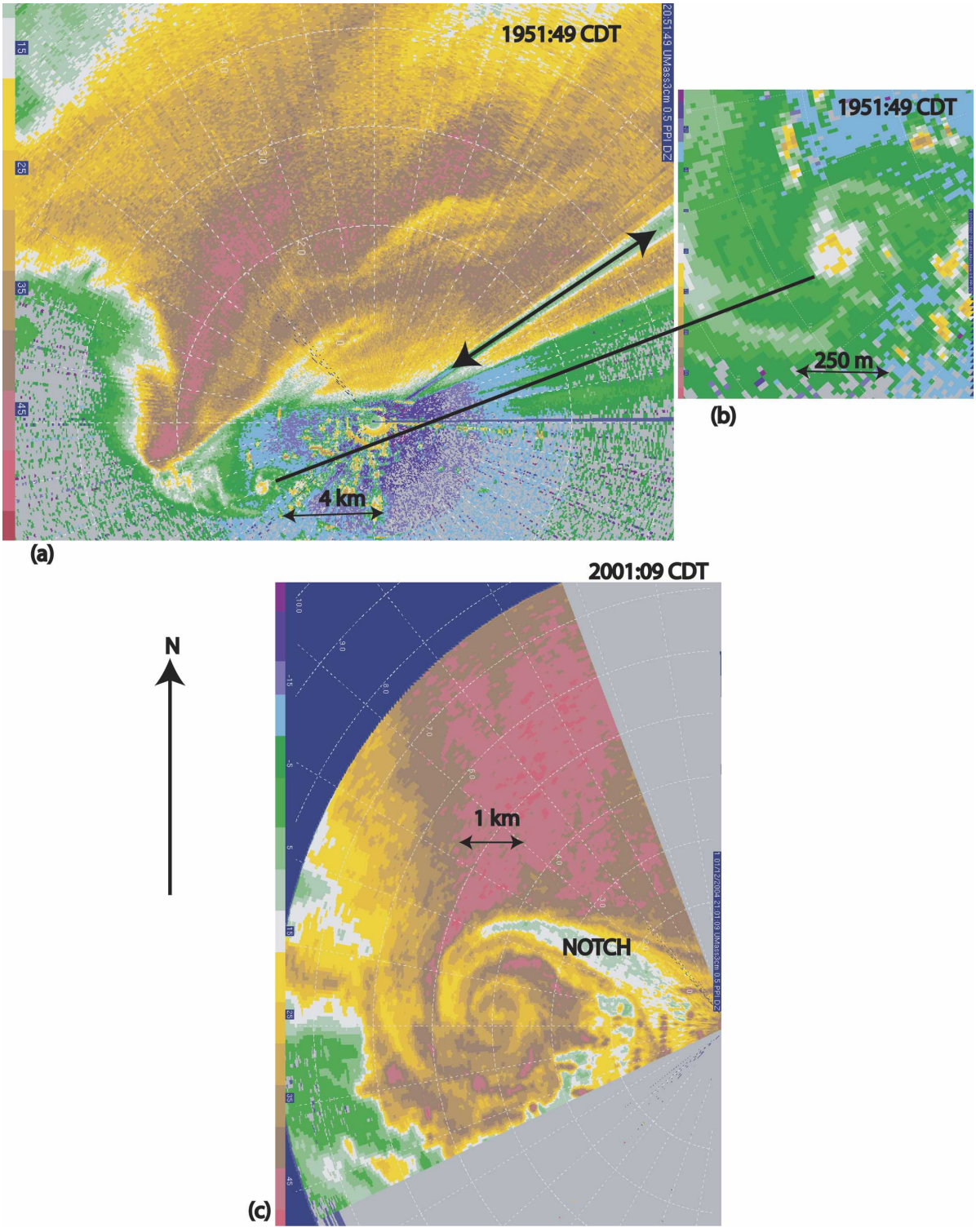

FIG. 3. Depiction of the radar reflectivity (dB*Z*, color coded at the left) of the Attica tornado, from data collected by the UMass, mobile, X-band Doppler radar (UMass X-Pol) at (a) 1951:49 CDT 12 May 2004, in "surveillance" mode; the entire parent supercell is shown; beam blockage is noted to the northeast (thick solid line with arrows on either end); (b) at 1951:49 CDT 12 May 2004, but inset for area around the tornado; slightly different color-scale increment from that used in (a); and (c) at 2001:09 CDT 12 May 2004, in "data-collection" mode; much of the parent supercell is shown. Range markings (white dashed lines) are shown in (a) every 4 km (range plotted in km/4), (b) every 250 m, and (c) every 1 km. The elevation angle was ~2.5°.

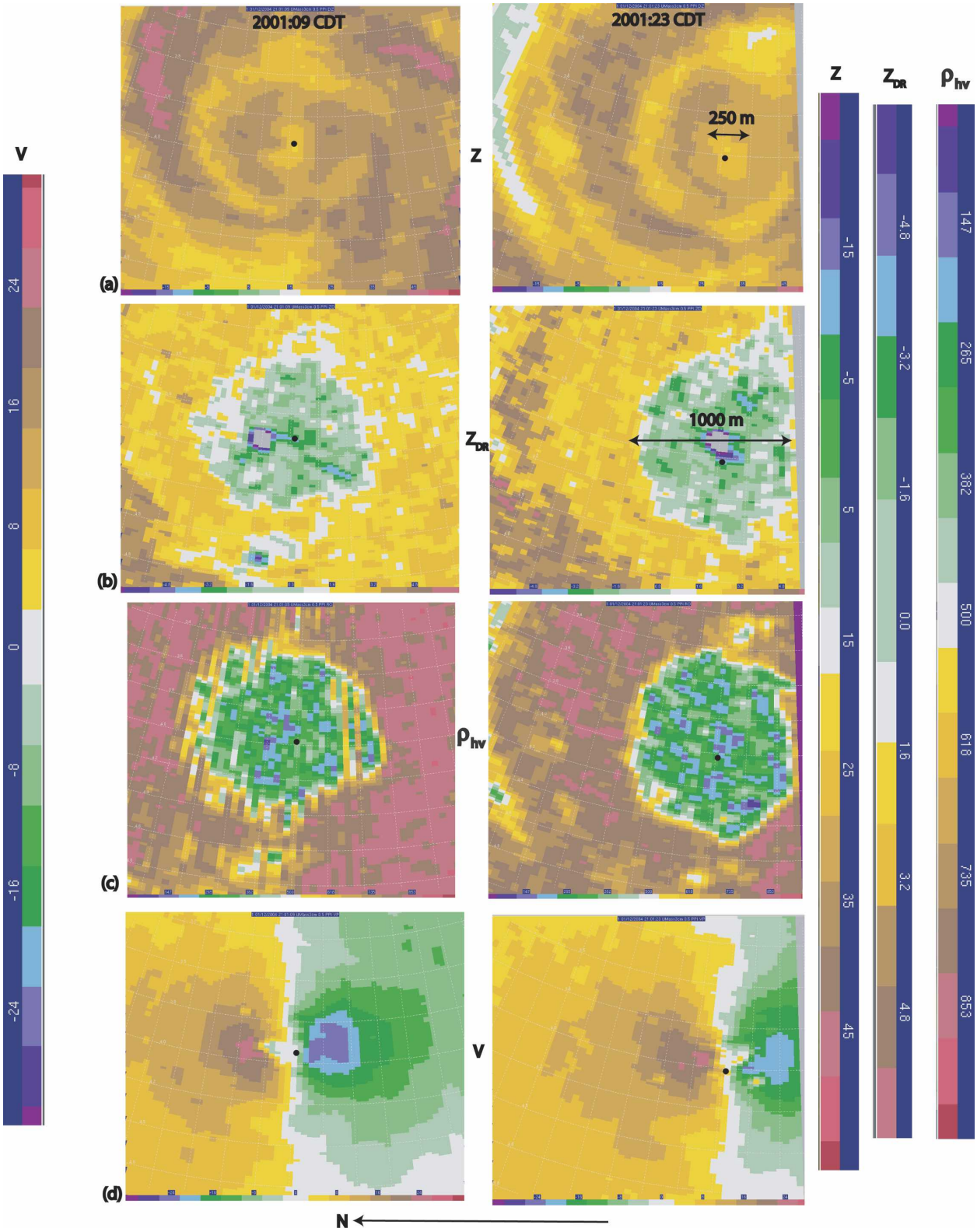

FIG. 4. Features of the tornado on 12 May 2004, just east of Attica, KS, as depicted by UMass X-Pol, but on a small scale just for the area in the vicinity of the tornado. (a) Radar reflectivity factor Z (dBZ), (b) differential reflectivity Z_{DR}, (c) cross-correlation coefficient ρ_{hv}, and (d) Doppler velocity V (m s^{-1}) at left (right) 2001:09 (2001:23) CDT. Range markers are displayed every 250 m [except in (b), where they are given every 200 m]; range marker values are given in km, but are truncated/rounded (so, e.g., 4.2 km is actually 4.25 km and 4.8 km is actually 4.75 km). Color codes for the scale of the parameters are shown at the bottom. Dot indicates the approximate location of the center of the tornado. Enlarged color scales are reproduced along the sides.

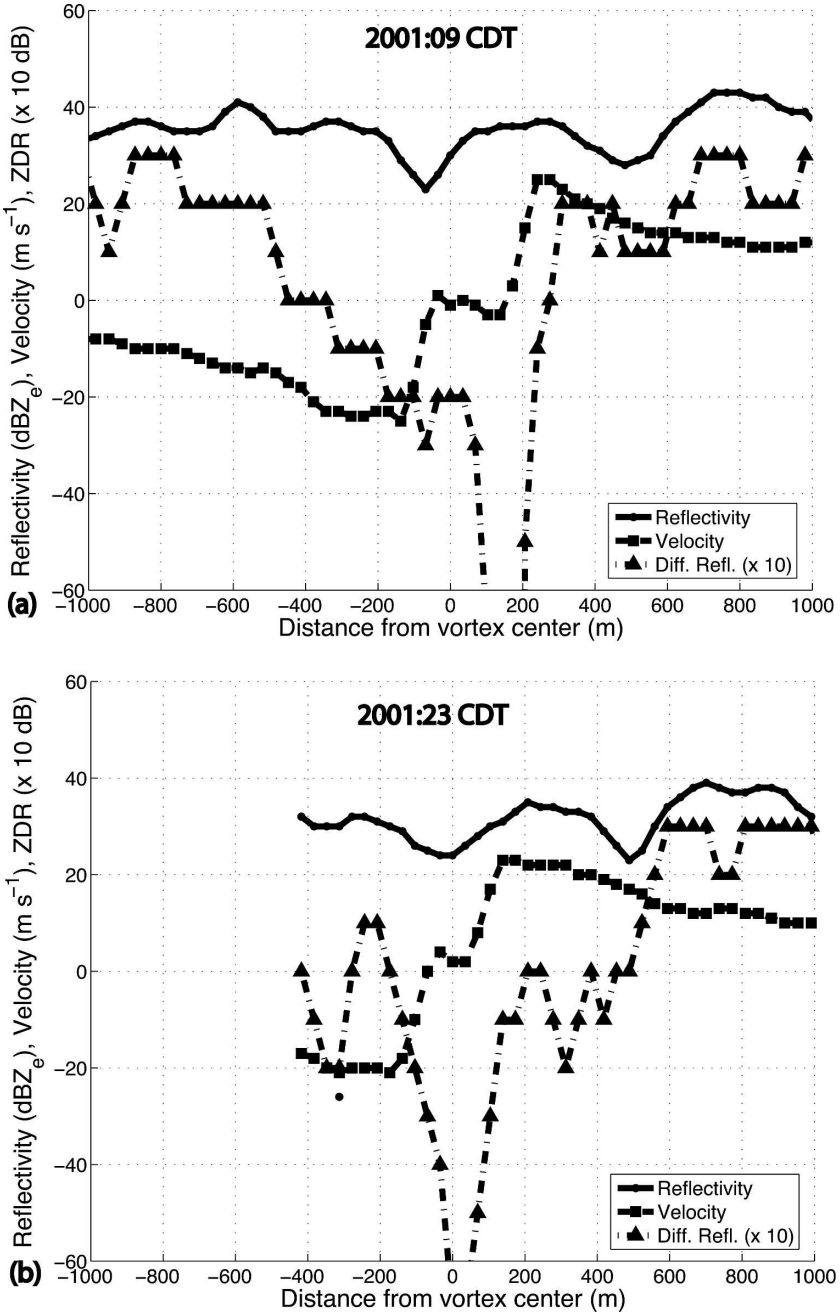

FIG. 5. Radial profiles of radar reflectivity (dBZ), Doppler velocity (m s^{-1}), and differential reflectivity Z_{DR} (dB $\times$ 10), during the mature stage of the Attica tornado. Profiles are from samples taken at a constant range, passing through the center of the tornado (denoted as a dot in Fig. 4). The distance from the vortex center is negative (positive) to the left (right) of the radar view of the tornado at (a) 2001:09 and (b) 2001:23 CDT.

than the distance to the radius of maximum wind speed (~160 m). It is thus concluded that the quasi-circular ring of intense reflectivity probably was composed of debris ($Z \sim 40$ dBZ and $Z_{DR} \leq 0.5$ dB) that were centrifuged radially outward (Snow 1984; Dowell et al. 2005), while the spiral bands were composed of hydrometeors ($Z \sim 40$–50 dBZ and $Z_{DR} \sim 1.5$–3 dB). However, since the sizes of the scatterers making up the debris cloud were not known, the centrifuging hypothesis cannot be tested in this case. Wurman et al. (1996) and Wurman and Gill (2000) had also suggested that, based on nonpolarimetric radar observations, the inner

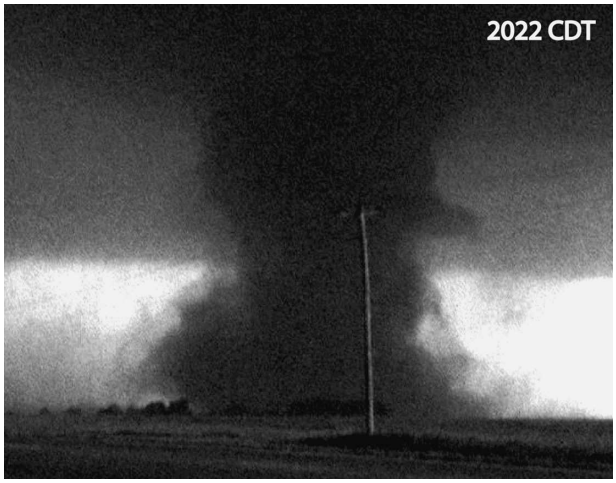

FIG. 6. Image of the tornado subsequent and to the east of the Attica, KS, tornado (the fourth tornado) at approximately 2022 CDT. Image is from a frame captured from a video. The view is to the southwest (cf. Fig. 1). (Image courtesy of H. Bluestein.)

ring of high reflectivity probably represents debris, while the outer spiral bands represent raindrops.

It is evident from the photograph shown in Fig. 2 that the debris cloud extended from the ground up to as high as ~600 m AGL. Wurman and Gill (2000) estimated the height of the debris cloud in a tornado to be ~700 m or greater. Unfortunately data were not collected at higher-elevation angles in our case so that variations of Z_{DR}, ρ_{hv}, and Z could not be correlated as a function of height. Since Ryzhkov et al. (2005) found a column of low Z_{DR} (<0 dB) as deep as 2 km in one case, it is believed that it is reasonable to assume that the column of debris would have been associated with a similar column of low Z_{DR}.

2) THE TORNADO SOUTHWEST OF HARPER

This tornado was rated only at F0, but had a much longer damage path than the Attica tornado (Fig. 1). Unlike the Attica tornado, this tornado moved to the east-northeast, and the storm-intercept crew therefore had to move periodically, to the east and then north to avoid getting too close to it. The tornado, though weak, still had a formidable-looking debris cloud (Fig. 6). Since Fig. 6 was made from a video frame capture and there were uncertainties in the focal length of the lens and the location, it was not possible to photogrammetrically analyze the visible debris/cloud width, etc., as in Fig. 2.

A storm-scale perspective of the radar reflectivity pattern of the 12 May supercell at the time of the tornado seen in Fig. 6 is shown in Fig. 7. A hook echo, the tip of which contains a small ring surrounding a pinhole, and a low-reflectivity notch north and northeast of the hook echo, are connected to the main body of the storm, which lies to the north and northeast.

As in the Attica tornado, the tornado seen in Fig. 6 was collocated with a ring of moderate reflectivity (~30 dBZ) and a vortex signature (brown to green couplet) with Doppler velocities as high as only ~25 m s^{-1} (Figs. 8a,c). In the 16 s between scans, the reflectivity pattern changed noticeably: the pinhole seen at 2021:28 CDT had filled in by 2021:44 CDT and the reflectivity just to the east of the tornado in a spiral band had increased from ~40 dBZ (brown) to ~45 dBZ (pink).

Regions of $Z_{DR} < 0.5$ dB and $\rho_{hv} < 0.5$ ~250–325 m across spanned across the center of the tornado (Figs. 8b,c) and covered a region having $Z \sim 20$–30 dBZ, save for the pinhole at 2021:28 CDT. At 2021:28 CDT it covered the region of the 30-dBZ ring (Fig. 8a). The diameter of the most intense winds in the tornado Doppler-velocity couplet was ~250 m. The ring (~330 m in diameter) is therefore thought to have been composed of debris, some of it centrifuged outward, rather than hydrometeors. In addition, there were narrow, curved bands of $Z_{DR} < 0.5$ dB and $\rho_{hv} < 0.5$ in the spiral band to the northeast of the tornado at 2021:28 CDT and to the east of it at 2021:44 CDT. It is suspected that these bands were also composed of debris, since they had $Z < 45$ dBZ; however, it is also possible that they were composed of a relatively small number of hailstones. At 2021:44 CDT a region of anomalously high Z_{DR} (brown) ~4 dB and low ρ_{hv} (green) ~0.5 appeared just to the west of the tornado. The change from just 16 s earlier was marked. It was associated with the tip of the spiral band noted earlier, and the appearance of higher reflectivities in it. We attribute this region to the sudden onset of large raindrops, perhaps associated with a "rain curtain" spiraling around the tornado, or to the sudden lofting of debris.

As in the Attica tornado, radar reflectivity, Z_{DR}, and Doppler velocity (but not ρ_{hv}) were plotted through the tornado, at the constant range of the center of the tornado (Fig. 9). A region of near-zero Z_{DR} is clearly evident encompassing the core of the tornado at 2021:28 and 20021:44 CDT.

c. *Tornadoes on 29 May 2004 in central Oklahoma*

1) THE "GEARY–CALUMET" TORNADO

A supercell that formed in western Oklahoma amidst convective storms that had begun near the dryline, tracked eastward and produced several tornadoes, one whose damage track began to the northeast of Geary and northwest of Calumet, Oklahoma (R. Smith, NWS, Norman, 2005, personal communication). (More de-

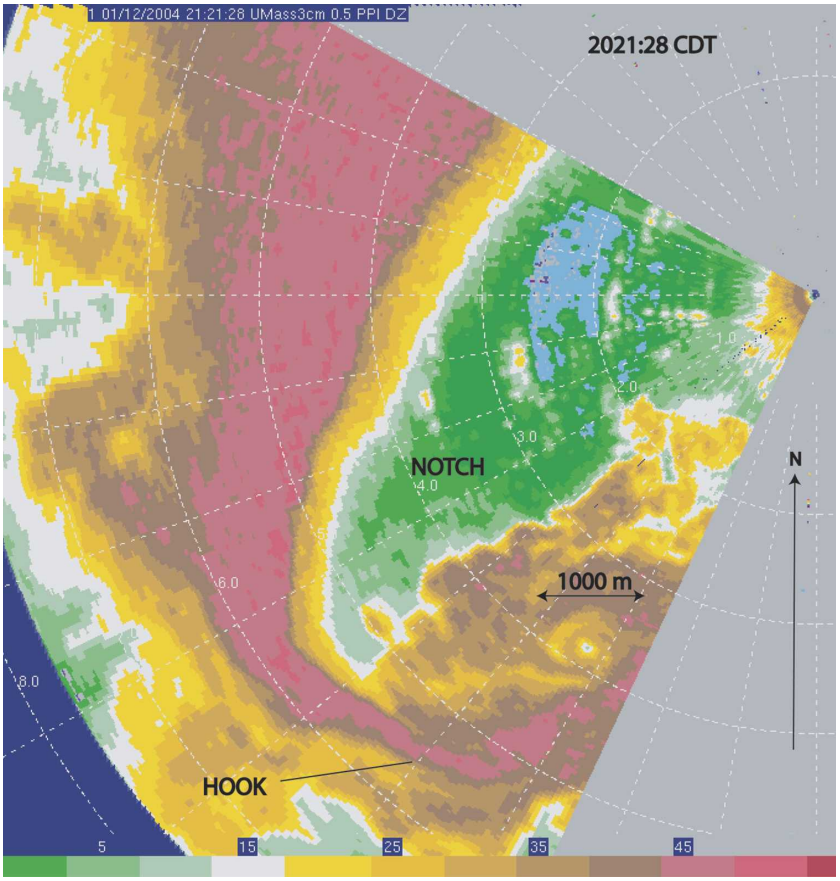

FIG. 7. Same as in Fig. 3, but for the tornado seen in Fig. 6, at 2021:28 CDT; the range markers are given in km. The elevation angle was ~3°. Radar was in "data-collection" mode.

tailed tornado track information can be found online at http://www.cswr.org/dataimages/rotate/geary-summary-2004-0711fp.pdf.) The "Geary–Calumet" tornado referred to in this section was named Tornado E in the aforementioned Web site. The damage path of the cyclonic tornado in Fig. 10 actually reflects the track of one of a number of tornadoes and/or parent mesocyclones. A detailed discussion of the evolution of all the vortices is beyond the scope of this study. The NWS rated the damage along the region of the tornado to the northwest of Calumet as F1, almost F2 intensity. This tornado was mostly hidden from view behind precipitation, but was visible to at least one storm chaser who was positioned in a favorable location with respect to it (J. Petrowski 2005, personal communication). From a vantage point north of Calumet, the storm was visible to the west-northwest as a striated cylinder having a flared-out base on its southern end (Fig. 11a). To the north of the base the sky was relatively bright. The storm looked very much like a high-precipitation (HP; Doswell et al. 1990; Moller et al. 1994) supercell (Fig. 11b) in that there was an extensive, dark-appearing area of precipitation underneath much of the base.

The radar depiction of the storm (Fig. 12a), however, deviated from the idealized depiction of an HP supercell (Fig. 12b). As in the HP model, the 29 May storm had an area of heavy precipitation behind the rear-flank gust front, south of the inflection point in the boundary that passed along the rear edge of the updraft. In the model, however, the area of precipitation to the rear of the rear-flank gust front is part of the main storm echo and curves such that the leading, eastern edge is concave, while in the 29 May storm the region of precipitation was convex, bulging forward; in addition, there was a narrow notch of weak reflectivity that curved around the leading edge of the precipitation, and this precipitation band circled an echo-weak hole or eye, that was connected to the main body of the storm's radar echo by a narrow band. Perhaps the reason why the 29 May storm deviated from the model was that the real storm had a much more intense cyclonic circulation (a tornado or tornado cyclone) than any cy-

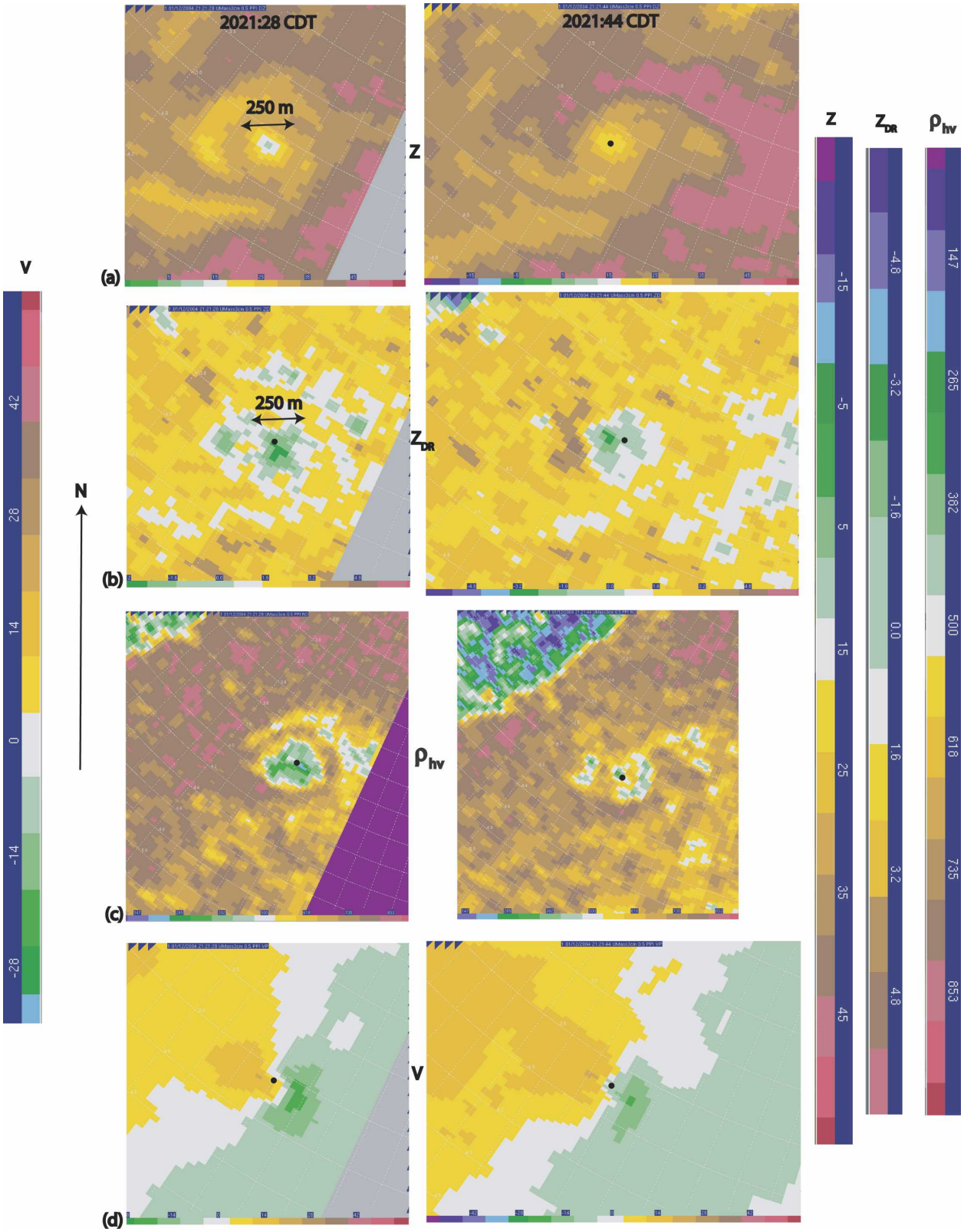

FIG. 8. Same as in Fig. 4, but for the tornado seen in Fig. 6, at left (right) 2021:28 (2021:44) CDT; (a) a dot is not plotted at 2021:28 so that the pinhole of light green at the center can be seen.

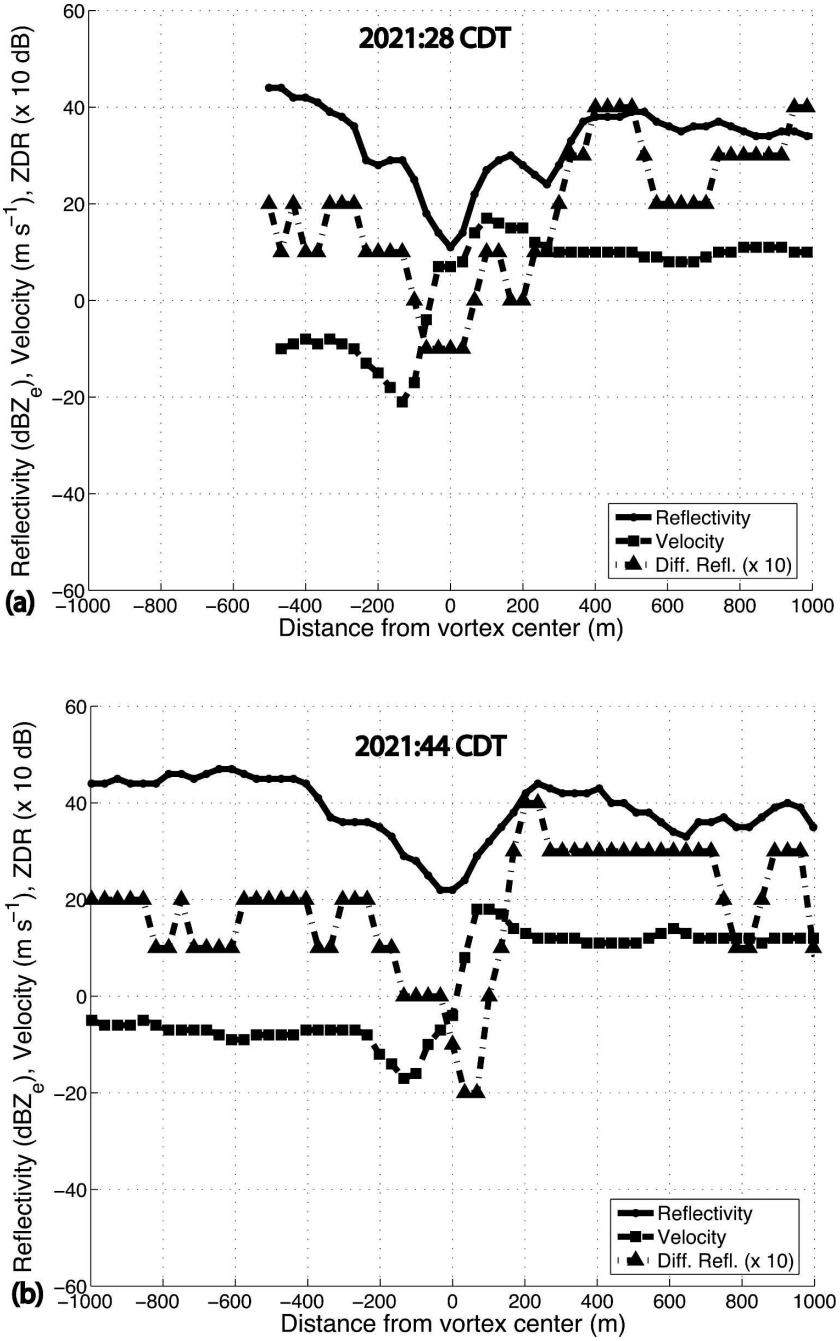

FIG. 9. Same as in Fig. 5, but for the tornado seen in Fig. 6 at (a) 2021:28 and (b) 2021:44 CDT.

clonic circulation implied in the model. The weak-echo notch seems to have been associated with the brighter area seen in Fig. 11, on the extreme right-hand (northeastern) side of the cloud base.

The radar reflectivity pattern associated with the tornado/parent circulation–mesocyclone northwest of Calumet and northeast of Geary was an echo-weak hole ~1.5 km wide at 1948:12 and 1950:07 CDT (Fig. 13a), and ~1 km wide at 1955:37 and 1957:17 CDT (Fig. 14a). The hole was embedded within a region of ~30-dBZ echo; higher reflectivities (~45 dBZ) were found to the southeast of the hole. At 1948:12 and 1950:07 CDT the width of the Doppler velocity vortex signature couplet was ~1.75 km (Fig. 13b) and had contracted to

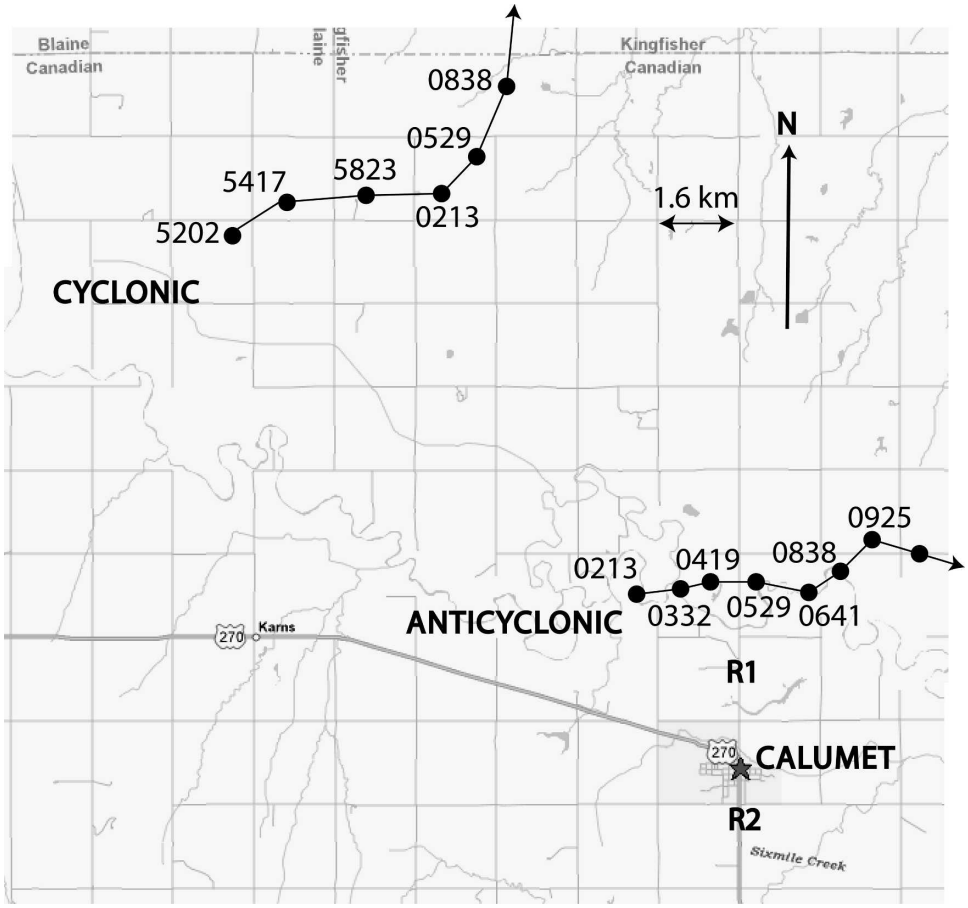

FIG. 10. Approximate tornado tracks of one of several cyclonic tornadoes near Geary, OK (to the west, off the map), and Calumet, OK, on 29 May 2004, as determined by the NWS, Norman, OK, and from tracks determined by a DOW radar. Also shown are the deployment sites (R1 and R2) of the UMass X-Pol. Base map adapted from Mapquest. Approximate times are given along the tracks in CDT as YYZZ, where the time in hours (as "19" or "20") is not shown, while YY and ZZ represent minutes and seconds, respectively. The second track was for one of several, rare, anticyclonic tornadoes. Damage in the track of the cyclonic tornado was rated as F1, almost F2.

~1.25 km at 1955:37 and 1957:17 CDT. Maximum Doppler velocities were ~28 m s^{-1} in the approaching direction; as in the Attica tornado, Doppler velocities were less than what one would expect in a tornado [according to the DOW Web site (http://www.cswr.org/dataimages/rotate/geary-summary-2004-0711fp.pdf) a tornado did not appear until 1952 CDT]. However, since the height of the radar beam was at least 925 m AGL, it is likely that the maximum wind speeds were at lower elevations and therefore not resolved. Because there was a lack of visual documentation of a tornado owing to an opaque region of precipitation, and because the vortex signature was so broad, the circulations at 1948:12 and 1950:07 CDT might be best characterized as strong mesocyclones.

The region within the core of the tornado/mesocyclone, which encompassed the weak-echo hole, Z_{DR} was <0.5 dB (Figs. 13b and 14b, light green region), except for an appendage of $Z_{DR} \sim 2$, which coincided with a curved band of reflectivity of ~20 dBZ that protruded inside the weak-echo hole at 1950:07 CDT (Figs. 13a,b, right side). It is possible that this feature was associated with precipitation that had been advected into the center of the circulation by a smaller scale vortex embedded within the hole. There is some evidence in the Doppler velocity field that there may have been a few submesocyclone-scale vortices (Fig. 13c, right side). However, this conclusion is not certain because the radar reflectivity pattern was weak at the edge of the hole where the smaller-scale vortices may have been and close inspection of the raw, unedited Doppler velocity data did not unambiguously support

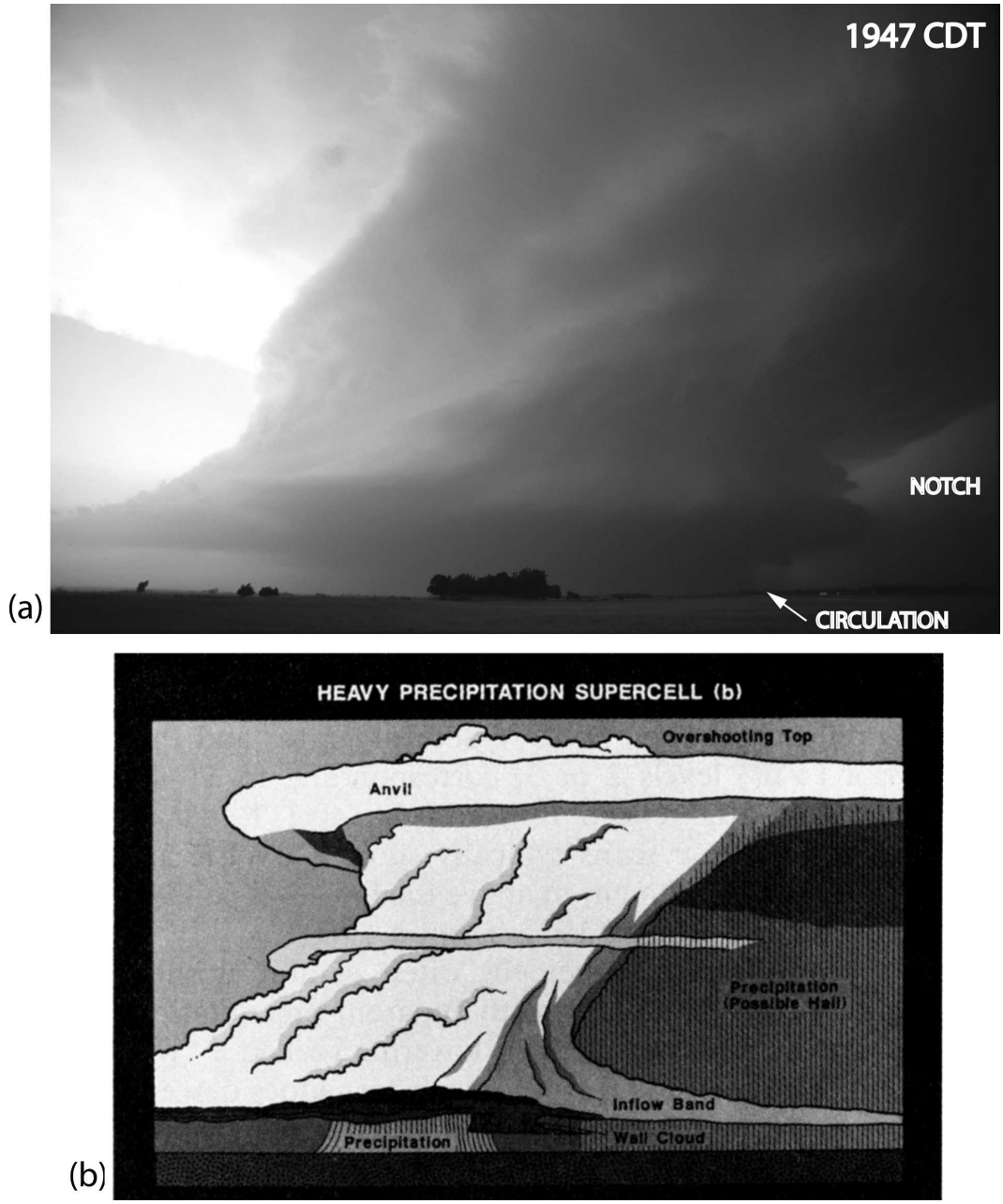

FIG. 11. (a) Photograph of the supercell near Geary, OK, on 29 May 2004, viewed from the east, 1.6 km north of Calumet, OK, at approximately 1947 CDT; wide-angle (17 mm) view is to the west (cf. Fig. 10). If there were a tornado present in the storm when (a) was taken, it would have been in the lower-right-hand sector of the image (denoted by "circulation"), hidden by precipitation. According to observations from the DOW (see online at http://www.cswr.org/dataimages/rotate/geary-summary-2004-0711fp.pdf), a tornado (noted "E") did not appear until 1952 CDT. (b) Idealized depiction of the cloud features in an HP supercell, from approximately the same vantage point as in (a). From Moller et al. (1994). (Photograph courtesy of H. Bluestein.)

the objective unfolding algorithm's analysis shown in the figure. It is not unlikely, though, that such a wide circulation could have been associated with multiple vortices (Davies-Jones et al. 2001), since widening of a vortex core can be associated with an increase in swirl ratio and a transition to a multiple vortex regime. There was no unambiguous association of a circular region of low Z_{DR}, however, and the tornado, as in the analyses of the tornadoes on 12 May 2004. In this case, a band of low Z_{DR} ($<$0.5 dB) (light green) from the rear (west)

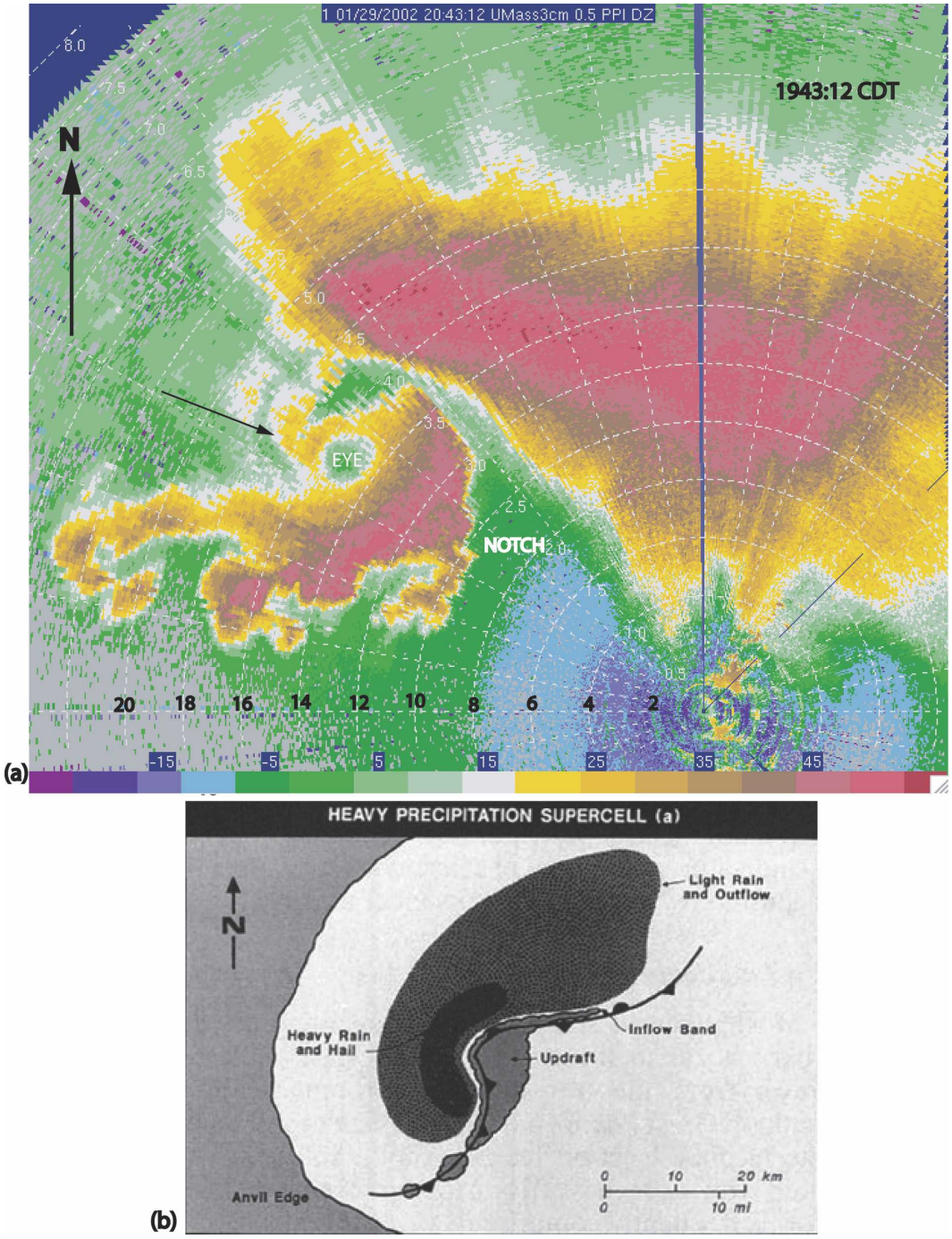

FIG. 12. (a) Storm-scale depiction of the radar reflectivity (dBZ) in the Geary–Calumet supercell at 1943:12 CDT 29 May 2004. Data were collected by UMass X-Pol in "surveillance mode." Range markings are given (in black) in km, every 2 km; the white range markers are shown every 2 km, with range plotted in km/4. The arrow points to a band of reflectivity that connects the main body of the storm to the "eye" and rear-flank gust front in the lower-left quadrant of the image. The "notch" of low reflectivity corresponds to the bright area seen in the lower-right portion in Fig. 11a. The lack of data in a narrow swath to the north of the radar is due to beam blockage. (b) Idealized plan-view depiction of radar-echo distribution, anvil edge, storm-induced surface boundaries, and storm updraft in an HP supercell. From Moller et al. (1994).

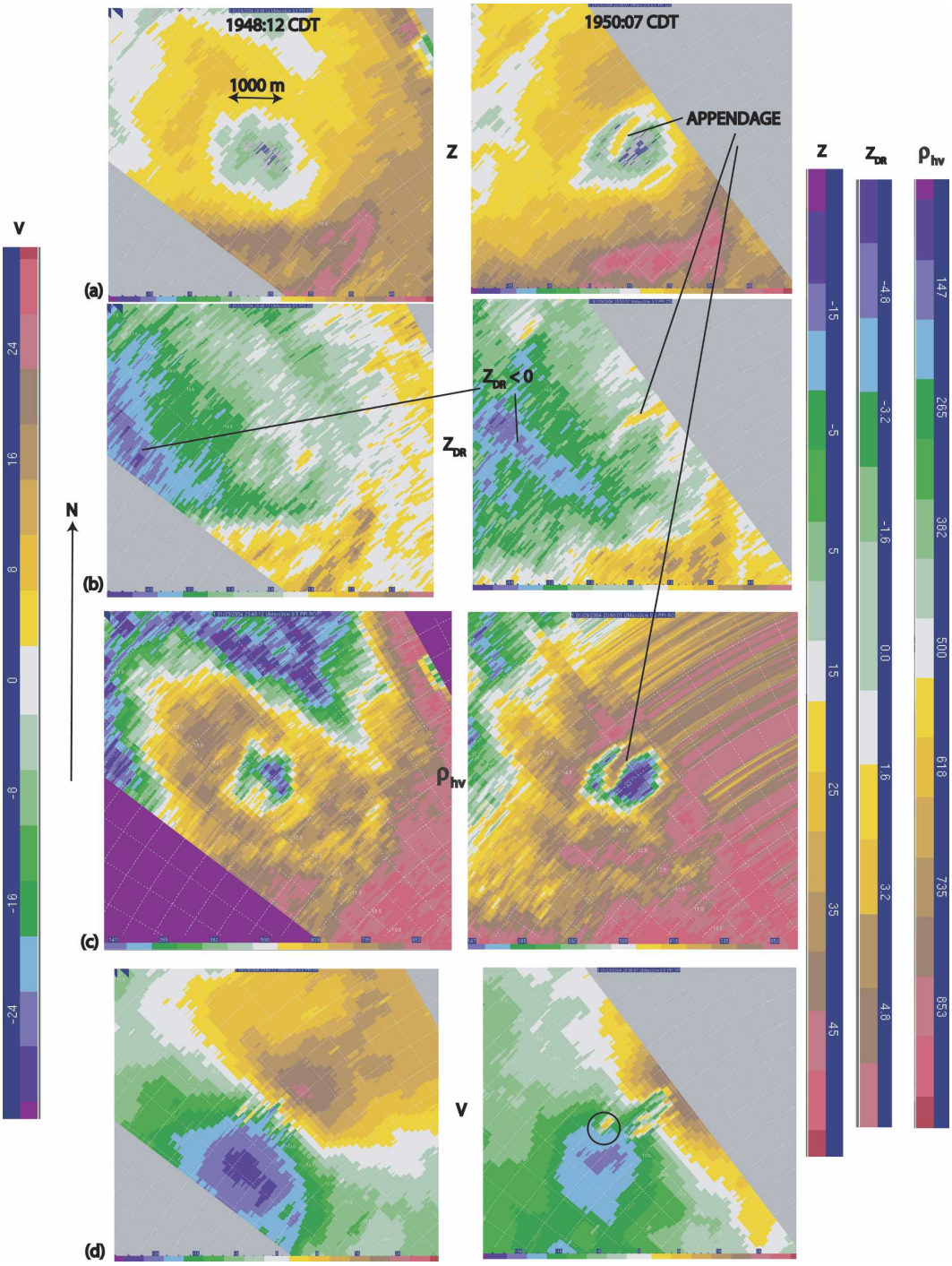

FIG. 13. Same as in Fig. 4, but for a mesocyclone northwest of Calumet, OK, at the left (right) 1948:12 (1950:07) CDT 29 May 2004, and with range markers shown every 500 m. Circle indicates a possible small-scale vortex signature.

connected with the region of low Z_{DR} near the core of the tornado. Part of this band of low Z_{DR} was significantly negative (as low as ~ -4 dB; purple) at 1948:12 and 1950:07 CDT. Ryzhkov et al. (2005) have also found negative values of Z_{DR} in a tornadic supercell; they attribute negative values to "a certain degree of vertical common orientation of the scatterers" or to "their large size." In this case, it is more likely that the

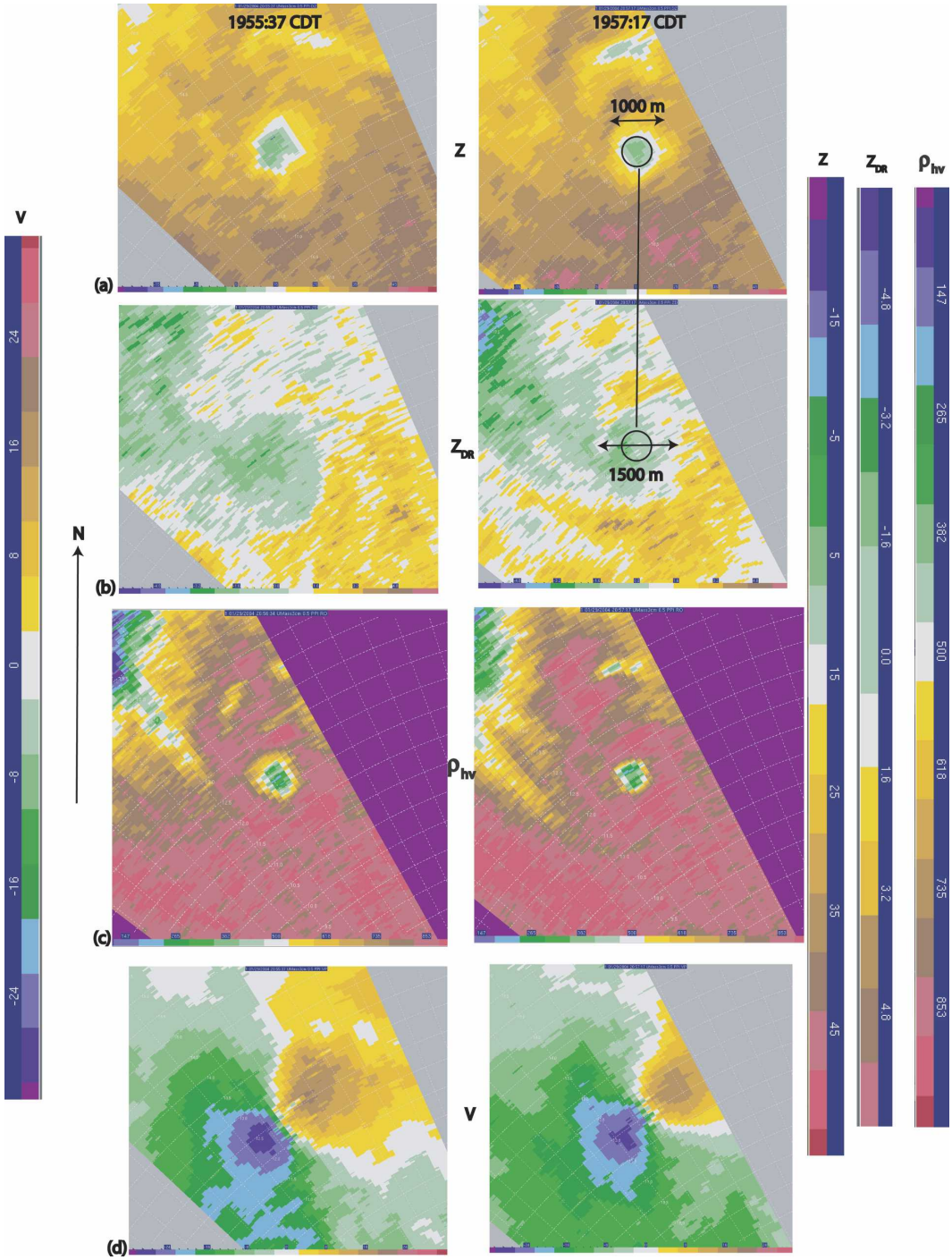

FIG. 14. Same as in Fig. 13, but for a tornado at 1955:37 (1957:17) CDT.

anomalously negative values of Z_{DR} were a result of differential attenuation because the radar beam would have passed through a region of high reflectivity (>50 dBZ; bright pink in Fig. 13a) before reaching the region of low Z_{DR}. Further evidence that these values of Z_{DR} were unrealistically low and due to differential attenuation is found in observations of ρ_{hv} (cf. Figs. 13b,c); values of ρ_{hv} are much too high to indicate debris. At 1955:37 and 1957:17 CDT there appeared to be a band of higher $Z_{DR} \sim 2$ dB wrapping around the region of weaker $Z_{DR} \sim 0.5$ dB or less (light green) that coincided with the center of the tornado. However, from

observations of ρ_{hv} (cf. Figs. 14a–c) it is seen that a region of $\rho_{hv} < 0.5$, which would be indicative of debris, has a diameter that is approximately the same as that of the weak-echo hole and is coincident with it, and so is therefore not likely significant.

2) THE ANTICYCLONIC "CALUMET" TORNADO

Following the deployment of UMass X-Pol to collect data just north of Calumet, the storm-intercept team retreated to a location just south of Calumet for safety, as the storm approached (Fig. 10). In a surveillance scan at 2003:54 CDT it is seen that the eye/weak-echo hole associated with the tornado northeast of Geary was still evident (Fig. 15a). At a low-elevation angle, where there was considerable blocking from utility poles and trees, an anticyclonic hook echo was seen ~10 km to the south-southeast of the eye. The weak-echo notch seen ~10–11 min earlier (Fig. 12) was still noted. About 1 min later, at 2004:58 CDT, the hole and anticyclonic hook are better seen (Fig. 15b), as the antenna had been elevated enough so that the radar beam was not being blocked by intervening utility poles and trees. The radar imagery in Figs. 15a,b look remarkably like that associated with the Grand Island, Nebraska, tornado of 3 June 1980 (Fujita 1981), in which a weak-echo hole was associated with a cyclonic tornado, and an anticyclonic hook, about 5 km away along the rear-flank gust front, was associated with an anticyclonic tornado. A similar flow pattern was inferred in a supercell in Iowa on 13 June 1976, which also produced a cyclonic–anticyclonic tornado pair (Brown and Knupp 1980).

Unfortunately, owing to a limitation of the signal-processing software, sector scans containing both the remains of the cyclonic tornado and the anticyclonic tornado in the 29 May storm were recovered in data-collection mode only at 2008:41 CDT (Fig. 16). It is seen that the remains of the cyclonic tornado were embedded within an area of a ~45–50-dBZ echo surrounding the center of the vortex (Fig. 16a), which was associated with a vortex signature couplet of only ~20–25 m s^{-1} of shear across the vortex couplet (Fig. 16c). The vortex was embedded within a region of $Z_{DR} \sim 1$–2 dB (Fig. 16b), which is indicative of precipitation, not debris. Furthermore, the ρ_{hv} in the region of the vortex was ~0.9, which is too high to indicate debris. Since data from a DOW indicated much stronger cyclonic shear (see online at http://www.cswr.org/dataimages/rotate/geary-summary-2004-0711fp.pdf), it is very likely the UMass radar beam sampled a volume well above the ground, where wind speeds associated with the tornado were much weaker.

A region of divergent, anticyclonic shear of ~18 m s^{-1} over 1 km (Figs. 16c,f) was located near the anticyclonic hook (Fig. 16a), more clearly seen in Fig. 15, several minutes earlier. No evidence of debris could be found in either Z_{DR} (Fig. 16b), which was too high, or in ρ_{hv}, which was also too high. Because there was no indication of debris and because the anticyclonic shear was too low, it is likely that as in the case of the cyclonic tornado to the north, the radar beam was above the column of strongest winds in the anticyclonic tornado.

At 2010 CDT an anticyclonic tornado appeared (Fig. 17) to the northeast of UMass X-Pol as a bright, sunlit condensation funnel (Fig. 10). A video taken by one of the authors (R. Tanamachi), who was located much closer to the tornado than UMass X-Pol, shows anticyclonically rotating clouds around the condensation funnel. In fact, the attention of our storm-intercept team was focused on the area of the remains of the cyclonic tornado to the north. It was a surprise to us that a new tornado formed where it did, because we were looking for a new cyclonic circulation and did not see one. The anticyclonic tornado discussed here is named Tornado F (see online at http://www.cswr.org/dataimages/rotate/geary-summary-2004-0711fp.pdf); another anticyclonic tornado named Tornado G was noted after UMass X-Pol stopped collecting data.

The visual evidence (Fig. 17), other storm chasers' accounts (e.g., see online at www.siue.edu/~jfarley/Chase%205-29-04.htm), the anticyclonic hook echo just a few minutes earlier, and Fujita's (1981) and Brown and Knupp's (1980) analyses also support the notion that the tornado in Fig. 17 was anticyclonic and had developed where the anticyclonic hook echo had been. More details concerning the anticyclonic tornadoes will likely appear in studies elsewhere that detail analyses of DOW and Shared Mobile Atmospheric Research and Teaching Radar (SMART-R) data.

4. Summary and discussion

Data in several supercell tornadoes in the Southern Plains, that had been collected by an X-band, dual-polarization, Doppler radar, were analyzed. It was found that regions of precipitation could be distinguished from regions of debris.

In one case (the "Attica" tornado), a debris ring was clearly evident as $Z_{DR} < 0.5$ and $\rho_{hv} < 0.5$ dB and $Z \sim 40$ dBZ, which was coincident with a Doppler signature of a cyclonic vortex. This finding was supported qualitatively by photogrammetric analyses of images of the tornado from the radar truck.

In another case (the tornado southwest of Harper, Kansas), an area of debris was indicated as a region (not a ring) of $Z_{DR} < 0.5$ dB, $\rho_{HV} < 0.5$, and $Z \sim 20$–30 dBZ (or less, with a narrow weak-echo hole at one

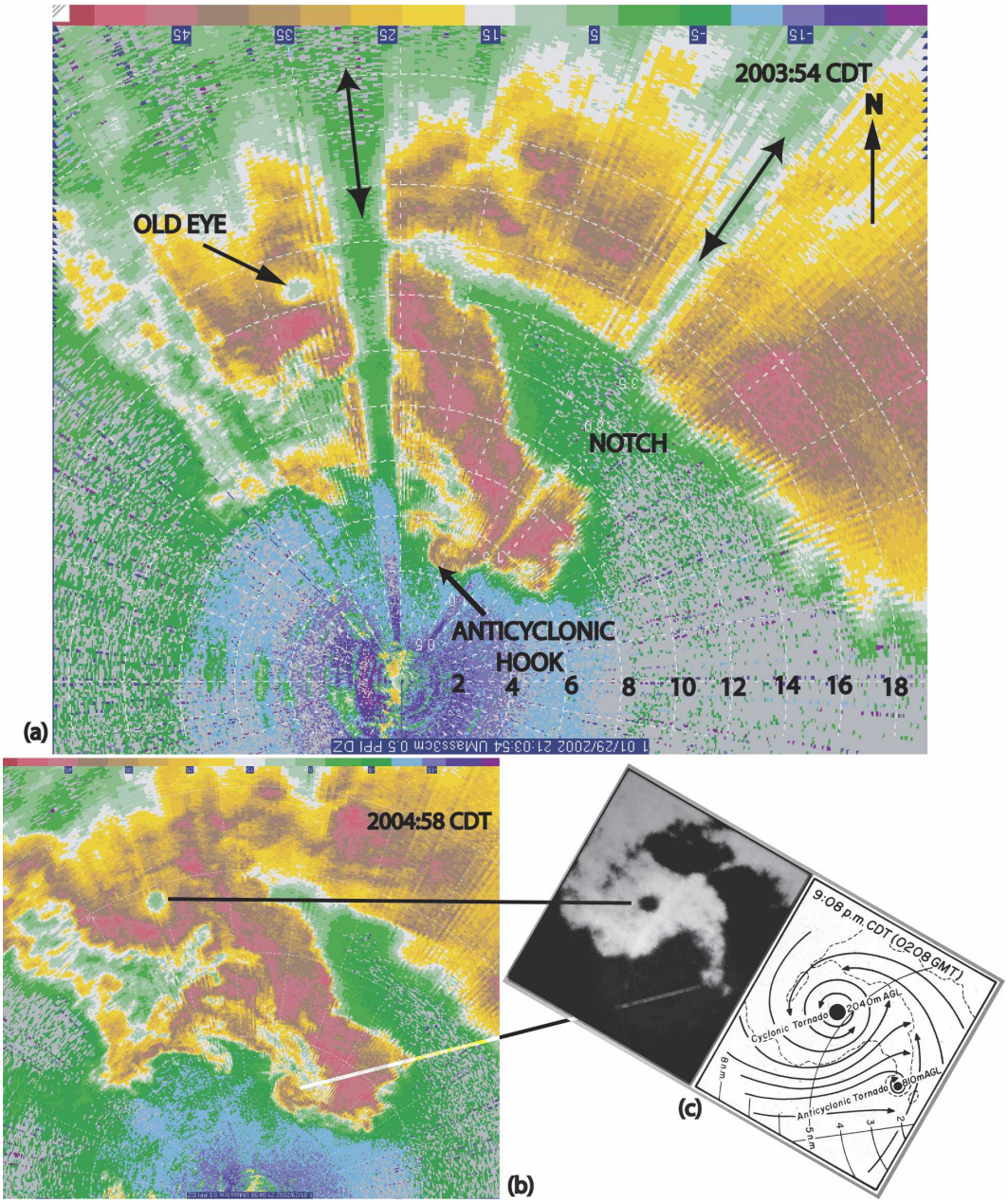

FIG. 15. (a) Same as in Fig. 12, but at (a) 2003:54 and (b) 2004:58 CDT. A rare, anticyclonic hook echo is noted. Two swaths of significant beam blockage are indicated by the thick solid-line segments with arrows at either end. (c) (above and to the left) WSR-57 radar reflectivity image of cyclonic and anticyclonic tornadoes to the northwest of Grand Island, NE, on 3 Jun 1980; from the NWS, Grand Island, NE; (below and to the right) estimate of streamlines about cyclonic and anticyclonic tornadoes at 2040 m and 810 m AGL, respectively, at 2108 CDT. From Fujita (1981). Corresponding weak-echo "eyes" and anticyclonic hooks are connected by lines.

time). In this tornado, a curved band of debris was noted near the tornado as a curved band of $Z_{DR} < 0.5$ dB, $\rho_{HV} < 0.5$, and $Z \sim 45$ dBZ.

In the "Geary–Calumet" tornado, which was not visible owing to intervening precipitation, the tornado was marked by a region of $Z_{DR} < 0.5$ dB and $Z \sim 25$–30 dBZ, outside of the inner, weak-echo hole. At one time, a band of low ($Z_{DR} < 0.5$ dB) and in one instance anomalously low, negative Z_{DR} (~ -4 dB) was located just to the southwest of the tornado in a region of moderately large Z ($\sim$30 dBZ). However, since ρ_{hv} was $>$0.5, it is likely that these regions did not have any

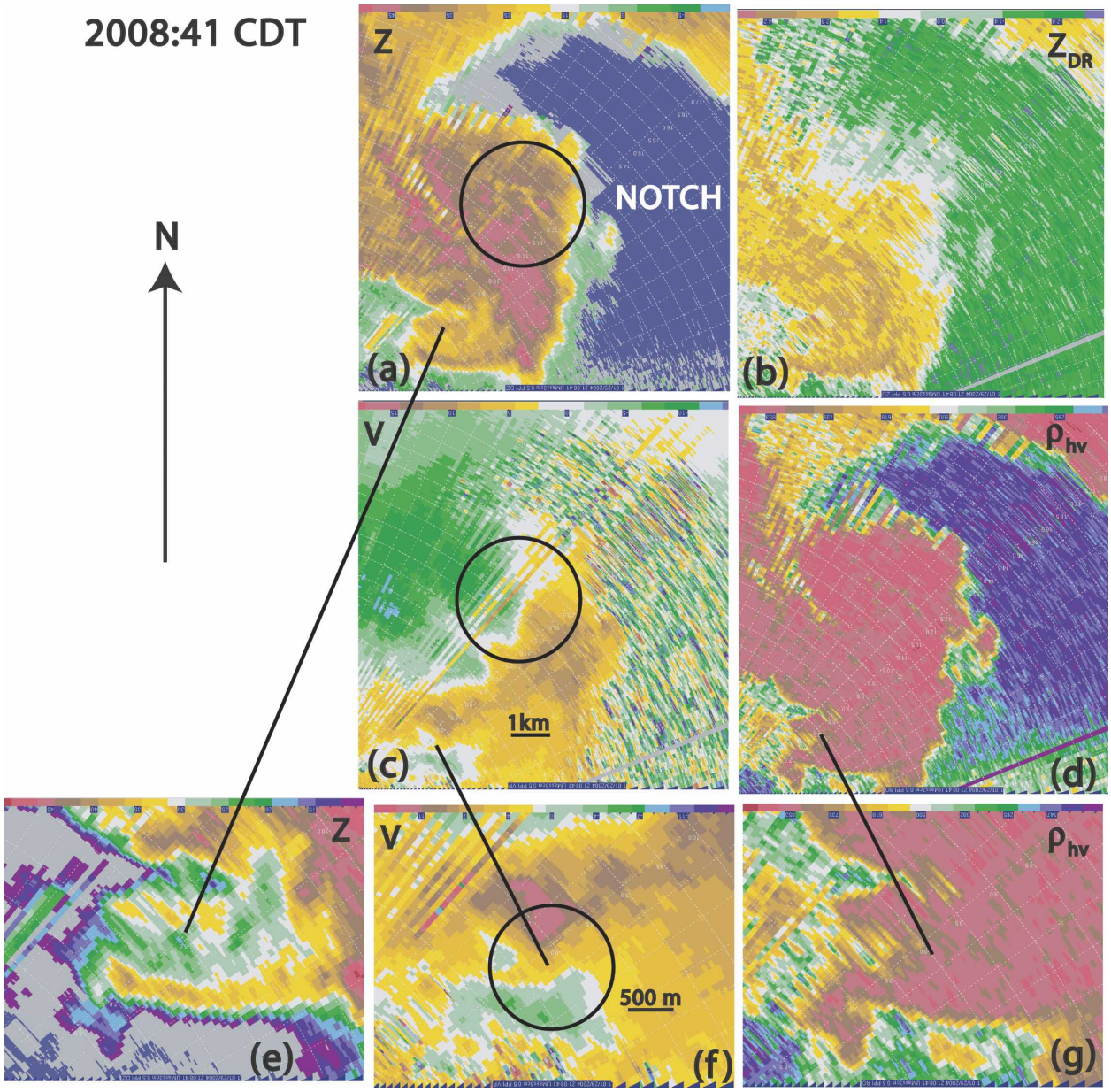

FIG. 16. Radar depiction from UMass X-Pol of a cyclonic–anticyclonic tornado–mesocyclone–mesoanticyclone pair at 2008:41 CDT 29 May 2004. (a) Radar reflectivity factor Z (dBZ), (b) differential reflectivity Z_{DR} (dB), (c) Doppler velocity V (m s^{-1}), and (d) cross-correlation coefficient ρ_{hv}. Circles in (a) and (c) denote the region of the cyclonic–vortex signature. (e) Expanded view of radar reflectivity factor in (a); color scale is different to enable the reader to see the pattern more easily. (f) Expanded view of Doppler velocity in (c); color scale is different to enable the reader to see the pattern more easily; circle marks location of anticyclonic vortex signature. (g) Expanded view of cross-correlation coefficient in (d). Range markers are displayed every 500 m; range marker values are given in km. Color codes for the scale of the parameters are shown at the top. In (a), the color scale is the same as that in Fig. 4a. In (b), light green is 0 dB, yellow is from ~1.5–~2.5 dB, and medium green is from ~−1.4 to ~−2.5 dB. In (c), brown is ~10–12.5 m s^{-1}, medium green is ~−7.5 m s^{-1}. In (d), the color scale is the same as that in Fig. 4c. In (e), yellow–brown are ~32–40 dBZ. In (f), pink represents ~11–13 m s^{-1}, medium green ~−7 m s^{-1}.

debris; the anomalously low values of Z_{DR} were probably due to differential attenuation. When attenuation is significant, it might be preferable to use ρ_{hv} rather than Z_{DR} to locate debris, since it is not sensitive to attenuation; it is, however, sensitive to differential phase, which is more likely in radar volumes that are not filled uniformly with the same type of scatterers, the same-sized scatterers, or are simply not completely

FIG. 17. Photograph of an anticyclonic tornado to the east-northeast of Calumet, OK, at 2010 CDT, viewed to the northeast from 1.1 km south of Calumet (cf. Fig. 10). (Photograph courtesy of H. Bluestein.)

filled with scatterers at all; it is expected that differential phase would be a problem in volumes where there are sharp gradients in reflectivity and/or when volumes are relatively large, such as at longer ranges. In future studies using dual-polarization radar data at X-band, it may be prudent to use both Z_{DR} and ρ_{hv} to distinguish not just debris from hydrometeors, but also different types of hydrometeors from each other. Future studies of dual-polarization, X-band radar data in tornadic storms might also benefit from corrections for attenuation using the "self-consistent" method of Bringi et al. (2001), as has been adapted for X-band data by Park et al. (2005a) and used by Park et al. (2005b).

It is therefore concluded, in accord with Ryzhkov et al. (2005), that dual-polarization radar data can help identify tornadoes by locating clouds of debris just above the ground. The analyses of data presented in this paper also support the identification of debris bands outside the center of a tornado.

The authors encourage more data be collected in and near tornadoes with mobile, dual-polarization, Doppler radars, along with detailed photographic documentation. In particular, more rapidly scanning and phased-array radars (e.g., Wurman and Randall 2001; PopSefanija et al. 2005) with full volume scans need to be used to obtain more complete analyses, which show the full three-dimensional structure of debris clouds.

Finally, since an anticyclonically rotating vortex–tornado, indicated as an anticylonic hook echo and in Doppler velocity as an anticyclonic shear signature, were found, it is hoped that numerical modelers can isolate the appropriate environmental conditions necessary for such a feature and simulate a supercell with a cyclonic–anticyclonic surface vortex–tornado couplet like those in the Geary–Calumet supercell. This rare type of storm is important because it can produce anticyclonic tornadoes in a region not focused on by spotters.

Acknowledgments. This work was supported by NSF Grant ATM-0241037 to OU and ATM-0242166 to UMass. The authors thank Mark Laufersweiler (OU) for his computer assistance. Rick Smith at the NWS in Norman, Oklahoma, provided damage-survey information for the 29 May storm. We are grateful to two anonymous reviewers for their comments, one of who located information from the DOW and SMART-R radars posted on public Web sites. The second author operated the radar in the field. Mark Laufersweilwer (OU) and Curtis Alexander (OU) assisted with computer- and graphics-related issues. Discussions with Guifu Zhang were helpful. Part of this work was done while the first author was a visiting scientist in the Mesoscale and Microscale Meteorology (MMM) Division at the National Center for Atmospheric Research (NCAR) in Boulder, Colorado. NCAR is supported by the National Science Foundation.

REFERENCES

Alexander, C. R., and J. Wurman, 2005: The 30 May 1998 Spencer, South Dakota, storm. Part I: The structural evolution and environment of the tornadoes. *Mon. Wea. Rev.,* **133,** 72–96.

Anagnostou, E. N., M. N. A. Anagnostou, W. F. Krajewski, A. Kruger, and B. J. Miriosvsky, 2004: High-resolution rainfall

estimation from X-band polarimetric radar measurements. *J. Hydrometeor.,* **5,** 110–128.

Bluestein, H. B., 1999: A history of storm-intercept field programs. *Wea. Forecasting,* **14,** 558–577.

——, and A. L. Pazmany, 2000: Observations of tornadoes and other convective phenomena with a mobile, 3-mm wavelength, Doppler radar: The spring 1999 field experiment. *Bull. Amer. Meteor. Soc.,* **81,** 2939–2951.

——, W. P. Unruh, J. LaDue, H. Stein, and D. Speheger, 1993: Doppler radar wind spectra of supercell tornadoes. *Mon. Wea. Rev.,* **121,** 2200–2221.

——, B. A. Albrecht, R. M. Hardesty, W. D. Rust, D. Parsons, R. Wakimoto, and R. M. Rauber, 2001: Ground-based mobile instrument workshop summary, 23–24 February 2000, Boulder, Colorado. *Bull. Amer. Meteor. Soc.,* **82,** 681–694.

——, C. C. Weiss, and A. L. Pazmany, 2003: Mobile Doppler radar observations of a tornado in a supercell near Bassett, Nebraska on 5 June 1999. Part I: Tornadogenesis. *Mon. Wea. Rev.,* **131,** 2954–2967.

——, ——, and ——, 2004a: Doppler radar observations of dust devils in Texas. *Mon. Wea. Rev.,* **132,** 209–224.

——, ——, and ——, 2004b: The vertical structure of a tornado near Happy, Texas, on 5 May 2002: High-resolution, mobile, W-band Doppler radar observations. *Mon. Wea. Rev.,* **132,** 2325–2337.

——, E. Holthaus, C. C. Weiss, S. Frasier, and A. L. Pazmany, 2005: High-resolution, mobile, W-band Doppler radar observations of the vertical structure of a tornado near Attica, Kansas on 12 May 2004. Preprints, *32d Conf. on Radar Meteorology,* Albuquerque, NM, Amer. Meteor. Soc., CD-ROM, P15R.2.

Bringi, V. N., and V. Chandrasekar, 2001: *Polarimetric Doppler Weather Radar: Principles and Applications.* Cambridge University Press, 636 pp.

——, T. D. Keenan, and V. Chandrasekar, 2001: Correcting C-band radar reflectivity and differential reflectivity data for rain attenuation: A self-consistent method with constraints. *IEEE Trans. Geosci. Remote Sens.,* **39,** 1906–1915.

Brown, J. M., and K. R. Knupp, 1980: The Iowa cyclonic–anticyclonic tornado pair and its parent thunderstorm. *Mon. Wea. Rev.,* **108,** 1626–1646.

Davies-Jones, R., R. J. Trapp, and H. B. Bluestein, 2001: Tornadoes and tornadic storms. *Severe Convective Storms, Meteor. Monogr.,* No. 28, Amer. Meteor. Soc., 167–221.

Doswell, C. A., A. R. Moller, and R. Przyblinski, 1990: A unified set of conceptual models for variations on the supercell theme. Preprints, *16th Conf. on Severe Local Storms,* Kananaskis Park, AB, Canada, Amer. Meteor. Soc., 40–45.

Doviak, R. J., and D. S. Zrnic, 1984: *Doppler Radar and Weather Observations.* Academic Press, 458 pp.

Dowell, D. C., C. R. Alexander, J. M. Wurman, and L. J. Wicker, 2005: Centrifuging of hydrometeors and debris in tornadoes: Radar-reflectivity patterns and wind-measurement errors. *Mon. Wea. Rev.,* **133,** 1501–1524.

Fujita, T. T., 1981: Tornadoes and downbursts in the context of generalized planetary scales. *J. Atmos. Sci.,* **38,** 1511–1534.

Junyent, F., A. L. Pazmany, H. B. Bluestein, M. R. Kramar, M. M. French, C. C. Weiss, and S. Frasier, 2004: Dual-polarization, X-band, mobile Doppler radar observations of hook echoes in supercells. Preprints, *22d Conf. on Severe Local Storms,* Hyannis, MA, Amer. Meteor. Soc., CD-ROM, P11.7.

Kosiba, K. A., R. J. Trapp, and J. M. Wurman, 2005: The 12 May 2004 Harper, KS, tornado: Analysis of DOW radar observations of the low level wind field. Preprints, *32d Conf. on Radar Meteorology,* Albuquerque, NM, Amer. Meteor. Soc., CD-ROM, P15R.11.

Kramar, M. R., H. B. Bluestein, A. L. Pazmany, and J. D. Tuttle, 2005: The "Owl Horn" radar signature in developing Southern Plains supercells. *Mon. Wea. Rev.,* **133,** 2608–2634.

Moller, A. R., C. A. Doswell III, M. P. Foster, and G. R. Woodall, 1994: The operational recognition of supercell thunderstorm environments and storm structures. *Wea. Forecasting,* **9,** 327–347.

Oye, R., C. K. Mueller, and S. Smith, 1995: Software for radar translation, visualization, editing, and interpolation. Preprints, *27th Conf. on Radar Meteorology,* Vail, CO, Amer. Meteor. Soc., 359–361.

Park, S.-G., V. N. Bringi, V. Chandrasekar, M. Maki, and K. Iwanami, 2005a: Correction of radar reflectivity and differential reflectivity for rain attenuation at X-band. Part I: Theoretical and empirical basis. *J. Atmos. Oceanic Technol.,* **22,** 1621–1632.

——, M. Maki, K. Iwanami, V. Bringi, and V. Chandrasekar, 2005b: Correction of radar reflectivity and differential reflectivity for rain attenuation at X-band. Part II: Evaluation and application. *J. Atmos. Oceanic Technol.,* **22,** 1633–1655.

Pazmany, A. L., F. Junyent, H. B. Bluestein, and M. Kramar, 2003: Quantitative rain measurements with a mobile, X-band, polarimetric Doppler radar. Preprints, *31st Conf. on Radar Meteorology,* Seattle, WA, Amer. Meteor. Soc., 858–859.

PopSefanija, I., J. Knorr, P. Buczynski, and R. Bluth, 2005: Advanced weather surveillance algorithms and techniques using a rapid scanning X-band radar—First results. Preprints, *32d Conf. on Radar Meteorology,* Albuquerque, NM, Amer. Meteor. Soc., CD-ROM, P12R.3.

Ryzhkov, A. V., T. J. Schuur, D. W. Burgess, and D. S. Zrnic, 2005: Polarimetric tornado detection. *J. Appl. Meteor.,* **44,** 557–570.

Snow, J. T., 1984: On the formation of particle sheaths in columnar vortices. *J. Atmos. Sci.,* **41,** 2477–2491.

Straka, J. M., D. S. Zrnic, and A. V. Ryzhkov, 2000: Bulk hydrometeor classification and quantification using polarimetric radar data: Synthesis of relations. *J. Appl. Meteor.,* **39,** 1341–1372.

Tanamachi, R. L., H. B. Bluestein, S. S. Moore, and R. P. Madding, 2006: Infrared thermal imagery of cloud base in tornadic supercells. *J. Atmos. Oceanic Technol.,* **23,** 1445–1461.

——, ——, C.-W. Lee, M. Bell, and A. Pazmany, 2007: Ground-based velocity display (GBVTD) analysis of W-band Doppler radar data in a tornado near Stockton, Kansas, on 15 May 1999. *Mon. Wea. Rev.* **135,** 783–800.

Wakimoto, R., W.-C. Lee, H. B. Bluestein, C.-H. Liu, and P. H. Hildebrand, 1996: ELDORA observations during VORTEX 95. *Bull. Amer. Meteor. Soc.,* **77,** 1465–1481.

Wurman, J., and S. Gill, 2000: Finescale radar observations of the Dimmit, Texas (2 June 1995) tornado. *Mon. Wea. Rev.,* **128,** 2135–2164.

——, and M. Randall, 2001: An inexpensive, mobile, rapid-scan radar. Preprints, *30th Int. Conf. on Radar Meteorology,* Munich, Germany, Amer. Meteor. Soc., CD-ROM, P3.4.

——, J. M. Straka, and E. N. Rasmussen, 1996: Fine-scale Doppler radar observations of tornadoes. *Science,* **272,** 1774–1777.

——, J. Straka, E. Rasmussen, M. Randall, and A. Zahrai, 1997: Design and deployment of a portable, pencil-beam, pulsed, 3-cm Doppler radar. *J. Atmos. Oceanic Technol.,* **14,** 1502–1512.

Zrnic, D. S., and P. Mahapatra, 1985: Two methods of ambiguity resolution in pulse Doppler weather radars. *IEEE Trans. Aero. Electron. Syst.,* **4,** 470–483.

——, and A. V. Ryzhkov, 1999: Polarimetry for weather surveillance radars. *Bull. Amer. Meteor. Soc.,* **80,** 389–406.